JOURNAL OF VIROLOGY, Sept. 2002, p. 8808–8819 Vol. 76, No. 17
0022-538X/02/$04.00+0 DOI: 10.1128/JVI.76.17.8808–8819.2002

Grapevine Fanleaf Virus Replication Occurs on Endoplasmic Reticulum-Derived Membranes

C. Ritzenthaler, C. Laporte, F. Gaire,† P. Dunoyer, C. Schmitt, S. Duval, A. Piéquet, A. M. Loudes, O. Rohfritsch, C. Stussi-Garaud,* and P. Pfeiffer

Institut de Biologie Moléculaire des Plantes, 67084 Strasbourg Cedex, France

Received 27 December 2001/Accepted 3 June 2002

Infection by *Grapevine fanleaf nepovirus* (GFLV), a bipartite RNA virus of positive polarity belonging to the *Comoviridae* family, causes extensive cytopathic modifications of the host endomembrane system that eventually culminate in the formation of a perinuclear "viral compartment." We identified by immunoconfocal microscopy this compartment as the site of virus replication since it contained the RNA1-encoded proteins necessary for replication, newly synthesized viral RNA, and double-stranded replicative forms. In addition, by using transgenic T-BY2 protoplasts expressing green fluorescent protein in the endoplasmic reticulum (ER) or in the Golgi apparatus (GA), we could directly show that GFLV replication induced a depletion of the cortical ER, together with a condensation and redistribution of ER-derived membranes, to generate the viral compartment. Brefeldin A, a drug known to inhibit vesicle trafficking between the GA and the ER, was found to inhibit GFLV replication. Cerulenin, a drug inhibiting de novo synthesis of phospholipids, also inhibited GFLV replication. These observations imply that GFLV replication depends both on ER-derived membrane recruitment and on de novo lipid synthesis. In contrast to proteins involved in viral replication, the 2B movement protein and, to a lesser extent, the 2C coat protein were not confined to the viral compartment but were transported toward the cell periphery, a finding consistent with their role in cell-to-cell movement of virus particles.

More than 30 years ago, it was suggested from electron microscopic and/or biochemical analyses that replication of positive-strand RNA viruses, whether in plants or in animals, takes place in association with intracellular membranes (for reviews, see references 13 and 14). The type of membranes involved in replication depends on the virus considered: tymoviruses, for instance, induce vesicular structures by invagination of chloroplast membranes in which both viral RNA and nonstructural proteins were detected (24, 25), whereas infection by tombusviruses leads to the formation of multivesicular bodies derived from mitochondria or peroxisomes (9, 56, 57). Several plant viruses belonging to different groups, such as tobamoviruses (30), bromoviruses (50), potyviruses (59), and comoviruses (11), similarly appear to strongly modify the endomembrane compartments. For *Cowpea mosaic virus* (CPMV), virus-induced accumulation of vesicles derived from the endomembrane system was described as early as 1974 by de Zoeten et al. (15), and in several instances fibrilar material tentatively identified as double-stranded RNA was shown to accumulate in such vesicles (20, 28). Viral proteins involved in replication were immunodetected on these vesicles in CPMV-infected cells (66). Similar information is available with animal viruses and has been described extensively in the literature, more particularly for poliovirus, the type member of picornaviridae. Evidence for the involvement of virus-induced vesicles in poliovirus replication was obtained already in the sixties (10), and the molecular mechanisms underlying the formation of virus-induced vesicles, their origin, and their role in viral replication were recently unraveled (19, 58, 62).

The fact that distinct types of membranes are involved in the replication of different viruses implies the establishment of specific interactions between such host membranes and virus-encoded proteins. In some cases, the transmembrane domains responsible for their anchoring on specific membranes could be identified (18, 35, 56) allowing the formation of dedicated structures where coupled translation and synthesis of both minus- and plus-strand RNA take place (8). Such complexes probably ensure protection of the viral RNA being synthesized from degradation by cellular RNases. In the case of poliovirus, it was shown that specific viral proteins were responsible for vesicle formation (6, 7, 62) and that formation of the poliovirus replication complex is a process that requires coupled viral translation, vesicle production, and viral RNA synthesis (19).

Grapevine fanleaf nepovirus (GFLV) has a bipartite RNA genome of positive polarity and, like all members of the *Comoviridae*, carries a small protein, VPg, covalently linked to the 5′ end of the viral genomic RNAs, which are both polyadenylated at their 3′ end. Each RNA encodes a single polyprotein, and this family of plant viruses shares therefore many common features with *Picornaviridae*. RNA1 encodes polyprotein P1 (253 kDa), which is processed by an embedded proteinase activity into five proteins required for replication, namely, 1A (of unknown function), 1B (probably the helicase), 1C (VPg), 1D (proteinase), and 1E (polymerase) (38, 40). These proteins are the only proteins required for RNA1 replication (65), and they function in *trans* to ensure RNA2 replication.

RNA2 encodes polyprotein P2 (122 kDa), which is pro-

* Corresponding author. Mailing address: Institut de Biologie Moléculaire des Plantes, 12 rue du Général Zimmer, 67084 Strasbourg Cedex, France. Phone: 33-3-88-41-72-00. Fax: 33-3-88-61-44-42. E-mail: christiane.garaud@ibmp-ulp.u-strasbg.fr.

† Present address: Ventana Medical System, 67400 Illkirch Graffenstaden, France.

cessed in *trans* by 1D into three proteins (39). Protein 2A is necessary for RNA2 replication, together with RNA1-encoded proteins (23). It is associated with membranous structures and is recruited by the RNA1-encoded replication machinery. We hypothesized that the 2A moiety of polyprotein P2 could mediate the transport of the nascent P2-RNA2 complexes from their initial location in the cytosol to the perinuclear replication sites where RNA2 replication and P2 cleavage take place (23). Therefore, protein 2A could play the role of a "homing protein." Protein 2B is the movement protein (MP) forming tubules through which viral particles are delivered to uninfected adjacent cells (54). Finally, protein 2C is the coat protein (CP).

Using epifluorescence microscopy, we have previously described the formation of a perinuclear complex where viral RNA was synthesized and viral proteins accumulated (23), but this could not be further analyzed due to technical limitations. In the present study, the structural preservation of cells and the intensity of immunolabelings were markedly enhanced, and image resolution was further improved by using high-resolution confocal microscopy. Moreover, the use of transgenic T-BY2 cell lines expressing green fluorescent protein (GFP) targeted to the endoplasmic reticulum (ER) and the Golgi apparatus (GA) provided a direct means to follow the virus-induced modifications of the endomembrane system and allowed us to conclude that GFLV replicates in association with specific membranes mainly derived from ER.

MATERIALS AND METHODS

Cell lines used for GFLV infection. Three tobacco T-BY2 cell lines were used throughout this study: a wild-type (wt) cell line and two transgenic cell lines accumulating GFP either in the ER (ER-GFP line) (44) or in the GA (Man1-GFP line) (45).

Antibodies. Polyclonal anti-VPg antibodies (named anti-VPg) were raised in rabbits against a synthetic peptide corresponding to the VPg sequence and purified by immunoaffinity chromatography against the VPg peptide (37). They were used at a 1/100, 1/300, or 1/5,000 dilution for immunosorbent electron microscopy (ISEM), immunofluorescence, and Western blot analysis, respectively.

For immunofluorescence microscopy, polyclonal anti-2B antibodies (named anti-MP) raised in rabbits as described in (53) were used at a 1:1,000 dilution; mouse monoclonal antibodies directed against 2C (named anti-CP) or against BrdU (Sigma) were used at a 1:500 dilution, and guinea pig polyclonal anti-double-stranded RNA (dsRNA) antibodies (36) were used at a 1:500 dilution.

The fluorescent conjugates Alexa-fluor-488 or -568 coupled to goat anti-rabbit, goat anti-guinea pig, or goat anti-mouse immunoglobulin G (IgG; referred to as A488 or A568, respectively) were from Molecular Probes (Eugene, Oreg.). They were used at a 1:300 dilution in phosphate-buffered saline (PBS) containing 0.1% (vol/vol) acetylated bovine serum albumin (BSAc; Aurion, Wageningen, The Netherlands).

For Western and dot blot analyses, mouse monoclonal antibodies directed against the ER retention motif HDEL (43) and rat monoclonal JIM84 Golgi-specific antibodies (31) were used at a 1/5,000 dilution.

Goat anti-rabbit IgG and goat anti-mouse IgG coupled to horseradish peroxidase were used as secondary antibodies at a 1/20,000 to 1/50,000 dilution and revealed by chemiluminescence (Lumi-Light Plus; Roche Diagnostics, Mannheim, Germany).

Preparation and infection of protoplasts. T-BY2 protoplasts were prepared from wt and transgenic cells from 4-day-old cultures. A total of 10^6 protoplasts were electroporated with 1 to 2.5 μg of viral RNA (100 Ω, 125 μF, 180 V) in a 0.4-cm cuvette and incubated at 27°C for 24 to 48 h as previously described (23). Mock-inoculated protoplasts (referred to as healthy protoplasts) were used as a control.

Sucrose gradient fractionation and analysis. One 10^6 protoplasts were harvested 72 h postinfection (hpi) and homogenized in 1 ml of modified buffer Q (59) containing 50 mM Tris-HCl (pH 8.0), 10 mM KCl, 3 mM $MgCl_2$, 1 mM EDTA, and 1 mM dithiothreitol and then supplemented with 0.1% bovine serum albumin (BSA), 0.3% dextran, 13% sucrose, 5 μg of leupeptin/ml, and 2 μg of aprotinin/ml. After a 10 min centrifugation at 4,000 × *g*, the supernatant was fractionated by centrifugation to equilibrium for 4 h at 29,000 rpm (SW41 Beckman Rotor) in a 11 ml of linear 20 to 45% sucrose gradient prepared in buffer Q containing 5 mM $MgCl_2$ (59). After centrifugation, 670-μl fractions were collected and analyzed by dot and Western blotting. For dot blot assays, 5-μl aliquots of each gradient fraction were spotted on two strips of Immobilon-P membrane (Millipore) and treated separately with anti-HDEL antibodies to localize ER-resident proteins or with JIM84 monoclonal antibodies for the detection of Golgi-specific glycosylation. For Western blot analysis, 15-μl aliquots of each fraction were fractionated by sodium dodecyl sulfate–12.5% polyacrylamide gel electrophoresis (SDS–12.5% PAGE), electrotransferred on Immobilon-P membrane, and immunoreacted with anti-VPg antibodies.

ISEM of sucrose gradient fractions. The procedure was adapted from Bienz et al. (7). Coating with immunoaffinity-purified anti-VPg antibodies was performed by floating Formvar-coated gold grids on drops of anti-VPg in PBS for 20 min, followed by three washes with PBS for 5 min. The grids were then floated for 15 min on a blocking solution (sonicated goat seric proteins from Roche at a 1/20 dilution in PBS) and washed again three times in PBS. The grids were incubated for 4 h at room temperature on 15-μl aliquots of the sucrose gradient fractions combined three by three, washed three times with PBS, and fixed for 5 min with 1% glutaraldehyde in PBS. After they were washed with bidistilled water, the grids were floated for 10 min on 0.1% (wt/vol) tannic acid, washed with water, postfixed for 10 min with 0.01% osmium tetroxide in water, dried, and finally observed under a Hitachi H600 electron microscope at 75 kV.

Immunolabeling of viral proteins. Infected protoplasts were harvested 24 or 48 hpi and fixed with 1% glutaraldehyde in culture medium (MS medium) for 15 min at room temperature (RT) under gentle agitation. The protoplasts were rinsed three times with MS and allowed to settle onto poly-L-lysine-coated coverslips and then treated three times (20 min, RT) with 500 μl of PBS containing freshly prepared 0.1% (wt/vol) sodium borohydride ($NaBH_4$) to permeabilize the cells and to reduce the autofluorescence induced by the glutaraldehyde. A blocking step was then performed for 1 h at RT in a solution consisting of PBS, 5% (wt/vol) BSA, 5% (vol/vol) normal goat serum, and 0.1% (vol/vol) cold water fish skin gelatin (Aurion). Cells were incubated overnight at 4°C in a moist chamber in the presence of the primary antibody at the adequate dilution in PBS-BSAc, washed four times in PBS, and further incubated in the dark for 4 h at RT with the adequate fluorescent conjugate in PBS-BSAc. Finally, cells were washed four times with PBS before confocal laser scanning microscopy (CLSM) observation.

Control experiments were performed with healthy protoplasts treated similarly or by using infected protoplasts incubated in the absence of primary antibodies to verify the specificity of the labeling.

Labeling and detection of nascent RNA. At 24 or 48 hpi, protoplasts were incubated for 1 h at 27°C with 10 μg of actinomycin D/ml to inhibit DNA-dependent transcription and then for 6 h with 100 μM BrUTP (Sigma) in the presence of 0.005% Triton X-100. Incorporation was stopped by the addition of the fixation medium (1% glutaraldehyde in MS), and the samples treated for immunolabeling as described above by using anti-BrdU antibodies (Sigma) and the adequate fluorescent conjugate.

BFA and cerulenin treatment. Immediately after electroporation, brefeldin A (BFA; Molecular Probes) or cerulenin (Sigma), both dissolved in dimethyl sulfoxide (DMSO), were added to the protoplasts culture medium to final concentrations of 10 and 30 μg/ml and of 30 and 45 μM, respectively. Protoplasts were further incubated for 48 h and harvested. Aliquots (20 μl) were treated with 0.1% fluorescein diacetate (FDA) to assess cell viability. Additional 300-μl aliquots were deposited on polylysine-coated slides that were then fixed by precipitation with acetone, rehydrated in PBS, and further immunolabeled with anti-CP or anti-VPg antibodies and the appropriate A568 and A488 conjugates as described above. The number of infected cells, as characterized by the presence of anti-CP and/or anti-VPg labeled structures, was counted versus the total number of protoplasts determined under UV illumination after staining the nucleus with Hoechst 33258.

Epifluorescence microscopy. Observations were done under an epifluorescence microscope Nikon Eclipse E800 with adequate filters. For FDA, the parameters were as follows: excitation wavelength (ex), 460 to 500 nm; dichroic mirror (dm), 505 nm; and emission long-pass filter, 510 nm. For A568, the parameters were as follows: ex, 515 to 565 nm; dm, 565 nm; and emission band pass filter, 582.5 to 627.5 nm. For Hoechst 33258, the parameters were as follows: ex, 330 to 380 nm; dm, 400 nm; and emission long-pass filter, 420 nm. Image acquisition was performed as previously described (23).

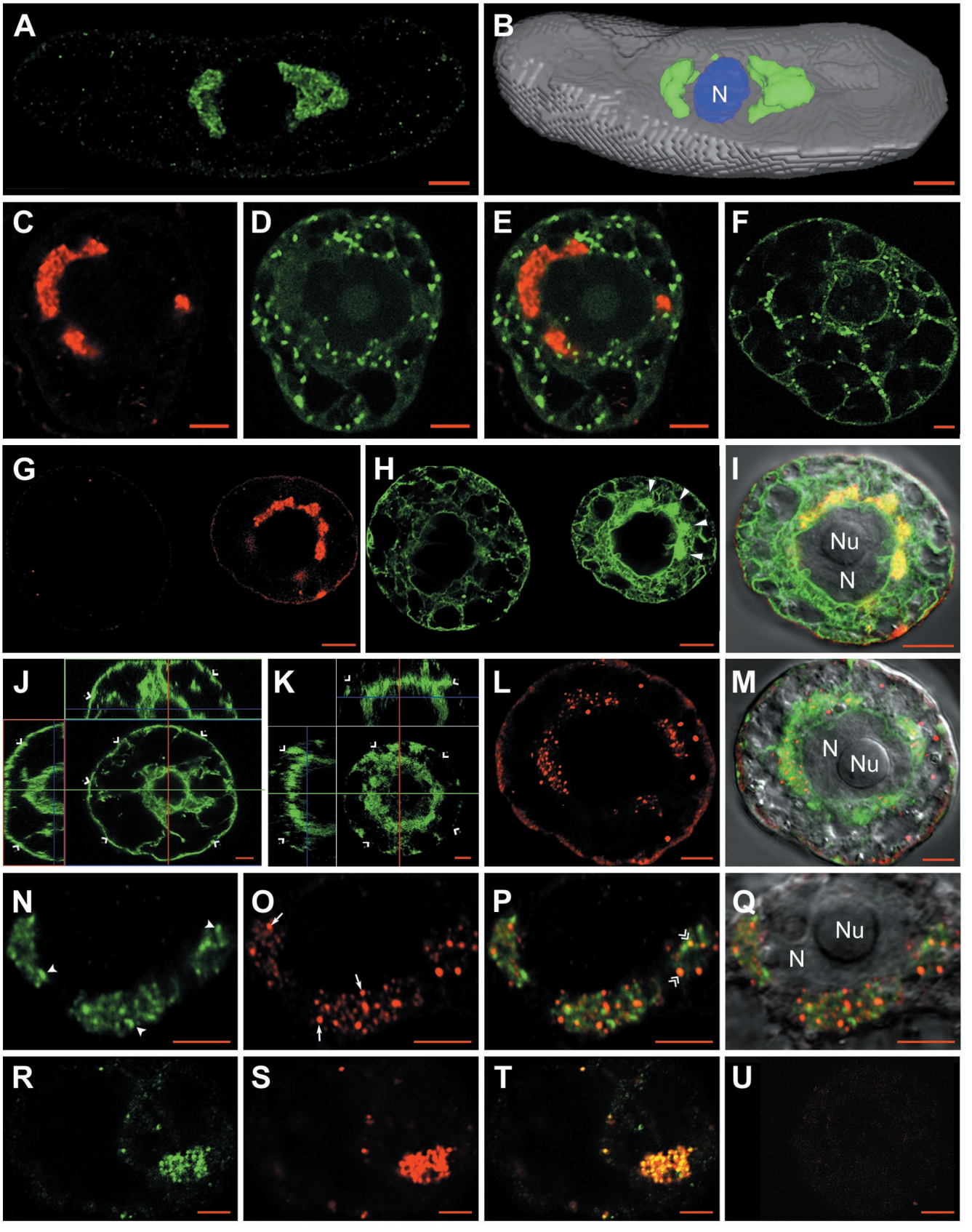

FIG. 1. Confocal immunomicroscopy on healthy or GFLV-infected T-BY2 protoplasts. The cell lines used were: wild type (A and B, N to U), transgenic cells expressing GFP targeted to the Golgi (C to F) or to the ER (G to M). Mock-inoculated and infected protoplasts were harvested

CLSM. For CLSM observation, cells were mounted in a chamber containing PBS–0.1% (wt/vol) sodium ascorbate (pH 7.4) to reduce photobleaching. Cells were observed with an inverted Zeiss Axiovert 100M microscope equipped with a LSM510 laser scanning confocal module and a ×63, 1.2 water immersion objective lens. Laser scanning was performed by using the multitrack mode to avoid cross talk.

Excitation and emission wavelengths were 488 and 505 to 545 nm, respectively, for either GFP or A488 and 543 and 560 to 633 nm, respectively, for A568. Image processing was performed by using LSM510 version 2.5 (Zeiss), and final image assembly was done with Photoshop 5.5 (Adobe Systems, San Jose, Calif.).

Three-dimensional reconstruction from CLSM image stack was obtained by using the surface rendering software (Bitplane, Zurich, Switzerland).

Protoplasts fixation and embedding for electron microscopy. At 48 h post-electroporation, protoplasts were fixed with glutaraldehyde as follows. An equal volume of 5% glutaraldehyde in 0.1 M phosphate (disodic monopotassic) buffer (PB), pH 7.2, containing 0.6 M mannitol was added to the medium. The protoplasts were maintained for 30 min at RT before centrifugation in an Eppendorf tube for 5 min at 40 × *g*. The fixative was replaced by 2.5% glutaraldehyde in 0.1 M PB and left for 40 min at RT. If necessary, the protoplasts were centrifuged (60 × *g* for 10 min) after glutaraldehyde fixation. After being washed with PB, the protoplasts were postfixed for 35 min at 4°C in 0.5% osmium tetroxide in the same buffer. They were washed (two 15-min washes) in distilled water, incubated at 40°C for 5 min, and mixed in an Eppendorf tube with the same volume of 2% low-gelling-point agar equilibrated at 40°C. After centrifugation (60 × *g* for 2 min at 37°C) and solidification of the agar at 0°C, the tube was sliced with a razor blade, and the extremity of the agar block containing the protoplasts was sectioned in small pieces (1 by 2 mm). These pieces were dehydrated in ethanol series and then in propylene oxide and finally embedded in standard Araldite-Epon medium (26). Staining and observations were as described elsewhere (55).

RESULTS

GFLV induces a redistribution of the ER but not of the GA to generate a perinuclear viral compartment where replication takes place. We have shown previously that the nonstructural RNA1-encoded proteins are the only viral proteins required for GFLV replication (65) and that at 48 h after transfection with GFLV-RNA, aggregates of RNA1-derived viral components accumulated around the nucleus. The structure and origin of these aggregates could now be resolved in much better detail by CLSM. Figure 1A shows that anti-VPg labeled polymorphous punctate-spongy perinuclear aggregates. These structures contained VPg either as a final maturation product or more likely as polyprotein precursors involved in RNA replication and could either take the shape of a ring or a cap or appear multilobed. They were variable in number and in size, and the perinuclear distribution of these VPg-containing aggregates could be clearly visualized in the three-dimensional reconstruction shown in Fig. 1B.

To investigate the possible involvement of ER and Golgi in the formation of these perinuclear aggregates, transgenic BY2 protoplasts expressing GFP either in the ER (ER-GFP) or in the GA (Man1-GFP) were electroporated with GFLV RNA. In Man1-GFP cells (Fig. 1C to F), infection by GFLV did not affect the GA, since distribution of the numerous round green spots corresponding to individual Golgi stacks was comparable in infected (Fig. 1C to E) and healthy (Fig. 1F) cells. However, Golgi stacks were never found in the VPg-labeled aggregates, as judged by the absence of yellow signal in the merged pictures (Fig. 1E), indicating that Golgi stacks were excluded from these areas. GFLV replication may nevertheless have more subtle effects on the GA during the course of infection: indeed, we occasionally noticed a decrease in the average number of Golgi stacks in infected cells that could reflect an (indirect) effect of GFLV replication on Golgi maintenance. Further in vivo time course analysis will be required to confirm the observed variations in the number of Golgi stacks within a single cell during the course of infection, but this is beyond the scope of this study.

As for Man1-GFP cells, infected ER-GFP protoplasts immunolabeled with anti-VPg (Fig. 1G to I) could be distinguished by their typical perinuclear labeling pattern (Fig. 1G, right cell). Anti-VPg labeling was found to be identical in either wild-type or transgenic T-BY2 cell lines (compare Fig. 1A, B, C, and G). No VPg aggregates were observed in control mock-transfected or uninfected protoplasts, as shown in Fig. 1G where a nonlabeled cell (left) is adjacent to an infected cell showing a strong label (right). A faint background signal due to the anti-VPg antibodies was occasionally found at the cell periphery (Fig. 1A and G). In contrast to Man1-GFP cells in which the GA remained essentially unaffected, the ER showed dramatic modifications in ER-GFP-infected cells. A profound alteration of the cortical network was observed, together with a marked condensation of the ER around the nucleus (Fig. 1H, right cell, large arrowheads). The ER aggregates and anti-VPg labeling colocalized perfectly as shown by the yellow signal obtained upon merging the two pictures (Fig. 1I). The modification of cortical ER and condensation of perinuclear ER (Fig. 1H) were never observed in uninfected cells, which all presented a typical ER distribution (compare Fig. 1H left with right cell). In extreme cases, GFLV infection resulted in the near depletion of the cortical ER. This phenomenon is particularly visible in Fig. 1K, representing an orthogonal projection of a series of optical sections taken from the top of an infected cell up to the equatorial plane through the nucleus (compare the orthogonal views from a healthy protoplast in which the cortical ER is clearly visible and indicated by open arrowhead in Fig. 1J with those from an infected one in Fig. 1K).

To demonstrate whether the ER-derived aggregates were involved in viral replication, double-labeling experiments were

at 24 hpi (R to U) or 48 hpi (A to Q). To monitor the synthesis of viral RNA, cells were fed at 24 hpi with BrUTP in the presence of actinomycin D and incubated for 6 additional hours to pulse-label the viral RNA (R to U). Cells were fixed with glutaraldehyde, permeabilized, quenched with $NaBH_4$, and treated with primary antibodies, followed by treatment with secondary antibodies coupled to fluorochromes (Ab1 and Ab2). Immunolabelings were performed with anti-VPg/A488 (A, B, N, P, and Q), anti-VPg/A568 (C, E, G, and I), anti-BrdU/A488 (R and T), and anti-dsRNA/A568 (L, M, O to Q, and S to U). Panels G and H show fields containing two adjacent cells; the left cell escaped infection and represents a healthy cell, whereas the right cell is infected and shows condensed ER (H; large full arrowheads). Panels J and K are orthogonal projections of two series of optical sections through a healthy cell with a typical cortical ER (J; single arrowheads) and an infected cell showing a depletion of the cortical ER (K; single arrowheads). Merged pictures were obtained by combining the green and red channels (E = C + D; I = G + H, right cells; M = K + L; P and Q = N + O; and T = R + S). The VPg-containing perinuclear aggregates and punctate dsRNA labeling are indicated in panel N by full arrowheads and in panel O by arrows. Colocalization between VPg and dsRNA labeling are designated by double arrowheads in panel P. Superposition of differential interference contrast in panels I, M, and Q allowed visualization of the cell content and, particularly, the nucleus. N, nucleus; Nu, nucleolus. Panels F, J, and U correspond to healthy cells. Bars, 5 μm.

performed with anti-dsRNA and anti-VPg antibodies. High-magnification CLSM observations again clearly revealed the typical punctate-spongy VPg labeling pattern (Fig. 1N). In contrast, dsRNA labeling (Fig. 1O, arrows) appeared as bright, discrete spots. These spots were always restricted to the VPg-labeled areas in the nuclear periphery (Fig. 1P) and were rather homogeneous in size, remaining individualized throughout infection. When superimposed, dsRNA and VPg labeling rarely coincided strictly, as judged by the very low number of yellow spots (Fig. 1P, double arrows) but were generally adjacent to each other. To confirm the assignment of dsRNA labeling to viral replication sites, newly synthesized viral RNA was traced by BrUMP incorporation in the presence of actinomycin D and compared to dsRNA labeling. Actinomycin D-insensitive incorporation of BrUMP into viral RNA was observed at the nuclear periphery, as assessed by the presence of small spots (Fig. 1R). The signals corresponding to newly synthesized RNA as traced by BrUMP incorporation (Fig. 1R) and the dsRNA template (Fig. 1S) colocalized perfectly (Fig. 1T). No significant signal was observed in similarly processed healthy protoplasts (Fig. 1U). Both dsRNA and BrUMP can therefore be considered as specific markers of viral replication sites.

Altogether, these results clearly confirm that GFLV replication occurs at numerous discrete sites associated with condensed ER (but not GA)-derived perinuclear aggregates. The intimate association between VPg accumulation sites and replication centers, as visualized by CLSM, strongly suggests that VPg (either fully processed or as a precursor) is a component of the viral replication complexes.

Ultrastructural analysis of the GFLV-induced perinuclear compartment. To further refine the analysis of GFLV replication sites, the ultrastructural organization of the perinuclear aggregates containing the viral products was studied by electron microscopy on infected protoplasts (Fig. 2). In contrast to uninfected cells, in which plastids and mitochondria were found surrounding the nucleus (Fig. 2A), the perinuclear area of cells at 48 hpi was densely packed with numerous electron-lucent to electron-dense vesicles that are variable in size (Fig. 2B and C, arrows) and that seemed to result from intense membrane proliferation, redistribution of endomembranes, and the fusion of vesicles. No electron-dense structures similar to those described in CPMV-infected cells (15) were observed. In addition, Golgi stacks were restricted to the periphery of these aggregates (Fig. 2B), a finding consistent with the CLSM observations (Fig. 1E). The perinuclear membrane proliferation areas observed in the electron microscope (Fig. 2) closely followed the distribution of GFLV replication sites revealed by CLSM (Fig. 1). It is thus very likely that these membranous structures corresponded to the ER-derived aggregates seen in CLSM and therefore to GFLV replication centers.

Additional ultrastructural alterations accompanied the modifications of the endomembrane system. Virus-like particles (Fig. 2C, small arrows) were often found trapped in bundles of filamentous material at the periphery of the vesicular aggregates (Fig. 2C, star). Such bundles of filamentous structures could not correspond to the previously described tubules made of the 2B movement protein and containing virions (54) since they were occasionally observed in healthy protoplasts (data not shown). Based on their diameter (ca. 11 nm), these bundles neither corresponded to microtubules nor to actin cables but were rather reminiscent of intermediate filaments (29), although evidence for their presence in plants remains scarce and rather inconclusive.

GFLV-induced vesicles cosediment with ER-resident proteins in sucrose gradients and can be immunocaptured by anti-VPg antibodies. To further characterize the GFLV-induced vesicles, crude extracts of healthy and infected T-BY2 protoplasts were fractionated in a linear sucrose gradient. Fractions were first analyzed by SDS-PAGE, followed by Western blotting with anti-VPg antibodies (Fig. 3A). No signal was detected in total protein extracts from healthy protoplasts (Fig. 3A, lane H). On the contrary, anti-VPg revealed several bands in total (Fig. 3A, lane I) and fractionated extracts from infected protoplasts (Fig. 3A, lanes 1 to 16). Four bands of VPg-containing precursors that migrated in the gel with apparent molecular masses of ca. 110, 90, 73, and 33 kDa were detected at the top of the gradient (Fig. 3A, lanes 1 and 2). Among these species, only the 73- and 90-kDa proteins clearly sedimented into the gradient (Fig. 3A, lanes 3 to 16). The sedimentation of Golgi (Fig. 3B) and ER markers (Fig. 3C) was revealed by the JIM84 and anti-HDEL antibodies: although it is notoriously difficult to resolve ER from Golgi markers in plants (47), the distribution of viral proteins recognized by anti-VPg antibodies, and singularly the 90- and 73-kDa VPg precursors, followed that of ER rather than Golgi markers. This result is in line with the association of GFLV replication with VPg precursors and with ER-derived membranes documented in Fig. 1 and 2.

In an attempt to visualize the membranes that cosedimented with the VPg precursors, ISEM was performed on sucrose gradient fractions with immunoaffinity-purified anti-VPg antibodies. Small vesicles were specifically immunotrapped by anti-VPg from ER-enriched bottom fractions of the sucrose gradient from infected protoplasts. No vesicular structures were immunocaptured from mock-infected protoplast fractions with purified anti-VPg antibodies (Fig. 4C), thus confirming the specificity of immunotrapping and the association of host membranes with VPg precursors. The trapping of vesicles was particularly pronounced in fractions 11 to 13, which proved to be highly enriched in vesicles ca. 80 to 120 nm in diameter (Fig. 4A, arrows). The external surface of the vesicles was systematically coated with electron-dense material (Fig. 4A). Both by their size and their morphology, these vesicles resemble the COP vesicles that traffic along the secretory pathway (1, 47). Some of these vesicles were aggregated into well-organized "rosette-like structures," as shown in Fig. 4B. Whereas the center of the rosettes was rather amorphous and electron dense, their periphery was made of vesicles similar in size to the isolated vesicles seen in Fig. 4A but smooth surfaced. Such rosettes were very reminiscent both in morphology and size to those isolated by ISEM from poliovirus-infected cells (4, 5).

Both BFA and cerulenin inhibit GFLV replication. The fungal metabolite BFA is known to inhibit exocytosis in a variety of eukaryotic cells (21, 33, 52) and to inhibit replication of viruses that require a functional secretory system such as poliovirus (12, 32, 42). In plants, BFA has been shown to block the secretion of cell wall polysaccharides and proteins (16, 34, 60). Recently, BFA was demonstrated to target Golgi-derived vesicles in tobacco BY2 cells, leading to the progressive for-

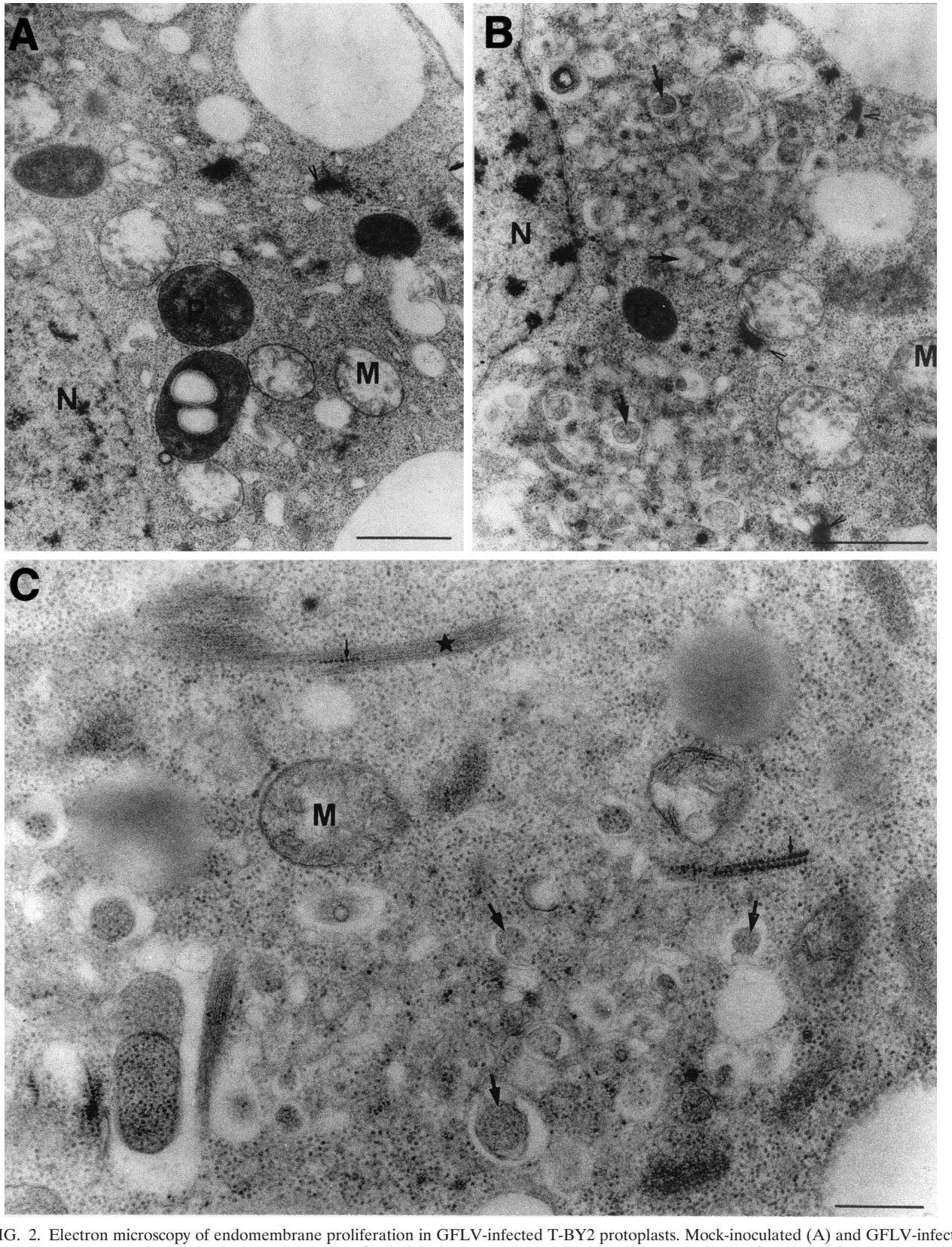

FIG. 2. Electron microscopy of endomembrane proliferation in GFLV-infected T-BY2 protoplasts. Mock-inoculated (A) and GFLV-infected (B and C) T-BY2 protoplasts were harvested at 48 hpi, fixed, dehydrated, and embedded in Epon. Ultrathin sections (90 nm) were stained with uranyl acetate and lead citrate. Note in panels B and C the abundance of small vesicles (arrows) near the nucleus in infected cells and in panel C the presence of virus-like particles (small arrows) trapped in filamentous material (star) located at the periphery of the vesicular aggregates. Arrowheads, Golgi; N, nucleus; P, plastids; M, mitochondria. Bars: 1 μm in panels A and B and 400 nm in panel C.

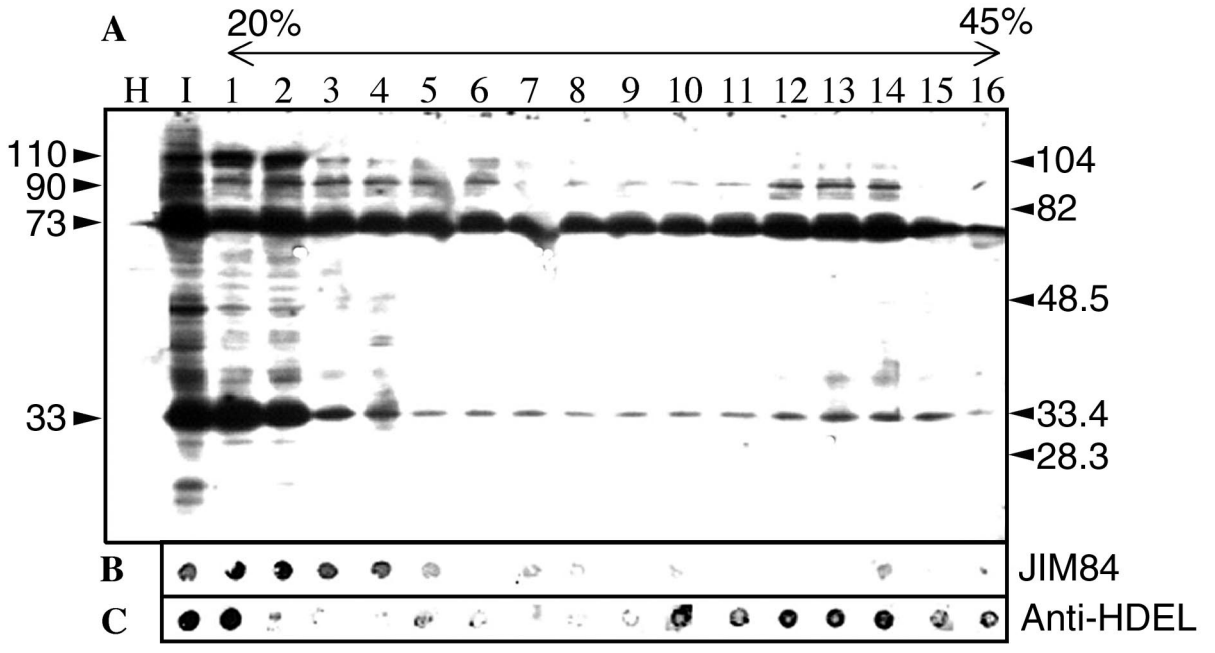

FIG. 3. Sucrose gradient fractionation of a crude extract of GFLV-infected T-BY2 protoplasts harvested at 72 hpi. Clarified crude extracts prepared from 10^6 protoplasts were fractionated by a 4-h centrifugation at 29,000 rpm through an 11-ml linear 20 to 45% sucrose gradient containing 5 mM $MgCl_2$. Sixteen fractions (670 μl each) were collected. (A) For Western blot analysis, 15-μl aliquots of each fraction were analyzed by SDS–12.5% PAGE, electrotransferred onto an Immobilon-P membrane, and then further immunoreacted with anti-VPg antibodies to reveal VPg-containing proteins. The molecular mass of protein standards are indicated in kilodaltons on the right side, and the apparent molecular masses of the VPg precursors are shown on the left side. (B and C) For dot blot assays, 5-μl aliquots of each fraction were applied as dots on two strips of Immobilon-P membrane (Millipore). The strips were treated either with JIM84 (B) or with anti-HDEL monoclonal antibodies (C). The membranes were then incubated with goat anti-rabbit IgG (A) or goat anti-mouse IgG (B and C) coupled to horseradish peroxidase and revealed by chemiluminescence.

mation of an ER-Golgi hybrid compartment (52). On the other hand, the antibiotic cerulenin targets the type II fatty acid synthase and is therefore a potent inhibitor of de novo lipid synthesis (48, 61). To test whether endomembrane integrity or membrane neosynthesis were essential for viral RNA replication, we analyzed the effects of BFA and cerulenin on GFLV replication (Fig. 5). Protoplast viability in the absence or presence of drugs was assessed 48 h after transfection by using FDA staining. The viability of freshly isolated protoplasts was in the 90% range and did not change significantly during the 48 h of incubation of mock- or GFLV RNA-electroporated protoplasts. Depending on the experiment, the addition of BFA resulted in a 10 to 40% decrease in viability in both cases, whereas the addition of cerulenin had virtually no effect. Due to the observed variation in protoplast viability, we chose to test the effect of the drugs on viral replication by calculating the percentage of infected cells as previously described elsewhere (11) rather than by Northern blot analysis. Therefore, mock-electroporated and infected protoplasts harvested at 48 hpi were processed for immunolabeling with anti-CP or anti-VPg antibodies. Because viral proteins accumulate to detectable levels only when replication takes place (23), the percentage of fluorescent cells was considered to correspond to the percentage of infected cells (between 400 and 1,000 cells were counted per experiment). To correct for variations in protoplast viability and percentage of infection between independent experiments, results were expressed as the ratio between the percentage of infection and the percentage of viable cells. This ratio was normalized to 100% for the infected samples incubated in the absence of drugs and to which only DMSO was added. Figure 5 shows the results of three independent experiments. Both BFA and cerulenin treatment resulted in a 30 to 70% decrease in infectivity depending on the concentration used. It can therefore be concluded that both de novo phospholipid biosynthesis and ER-Golgi integrity are required for efficient GFLV replication.

Viral proteins not involved in replication are not restricted to the virus-induced ER-derived compartment. To compare the distribution of the viral proteins involved in replication with that of proteins involved in movement and encapsidation, we analyzed the intracellular distribution of the movement protein 2B (MP) and the coat protein 2C (CP), both of which are dispensable for replication (23). Unlike VPg labeling, the intracellular coat protein distribution was not homogeneous in between cells. The 2C protein was predominantly found in the perinuclear viral compartment (Fig. 6B, C, E, and F, arrowheads), where it localized with condensed ER (Fig. 6A and C). Occasionally, very clear CP-labeled spike-like structures were detected within the cytoplasm (Fig. 6D). Finally, coat protein was also sometimes observed within the nucleoplasm (Fig. 6E to F, arrow) and as spots at the cell periphery (Fig. 6H). These spots proved to be localized at the tip of MP-labeled tubules (Fig. 6G, I, and J) and most probably corresponded to viral particles detected at the end of broken tubules. Since no CP labeling was observed along the intact part of the tubules, virions were probably inaccessible to antibodies there, as al-

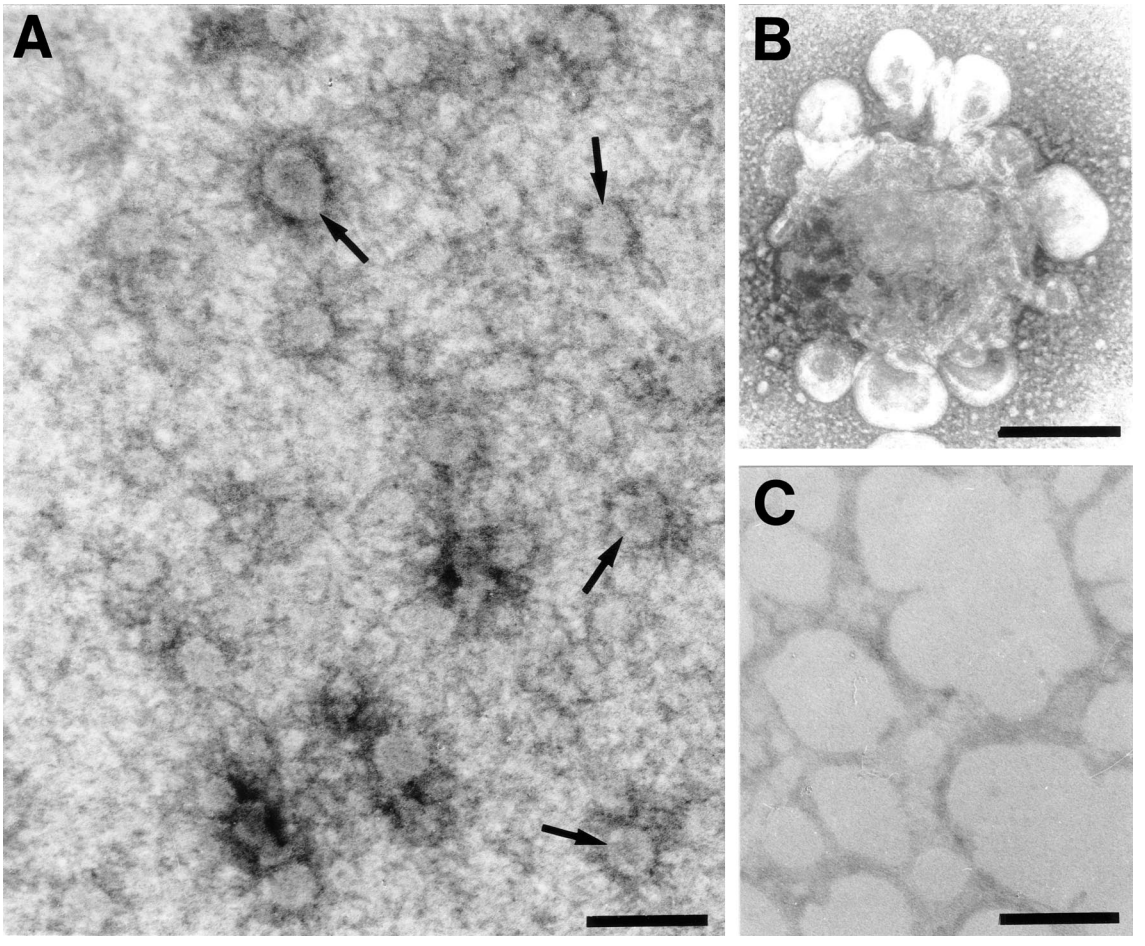

FIG. 4. Immunotrapping of vesicles obtained by sucrose gradient separation of crude extracts from GFLV-infected T-BY2 protoplasts harvested at 72 hpi (A and B) and healthy protoplasts (C). Formvar-coated electron microscopic grids were first coated with affinity immunopurified anti-VPg antibodies and then floated on aliquots of the gradient fractions combined three by three. The bound material was successively fixed with glutaraldehyde, tannic acid, and osmium tetroxide before observation under the electron microscope. Immunocapture of vesicles was observed only with bottom fractions 11 to 13 from infected samples. Vesicles were either isolated (A) or aggregated in rosette-like structures (B). Bar, 200 nm.

ready observed with CPMV (64). In spite of being derived from the same polyprotein as CP, the MP was rarely detected anywhere else than in tubules. When detected in the nuclear periphery, the MP signal appeared as small, round aggregates (Fig. 6K) that never localized strictly with that of CP (Fig. 6L and M).

DISCUSSION

Similarities and differences in the cytopathic effects induced by different plant viruses. Virus-induced accumulation and/or proliferation of membranes is a strategy commonly employed by RNA viruses to increase the available membrane surface area and to provide for the membranous structures they use as a scaffold to assemble their replicative machinery. GFLV infection resulted in an extensive redistribution of the ER that could be readily visualized and followed by CLSM in transgenic ER-GFP T-BY2 cells. The specific cytopathological effect of GFLV infection culminated in the nearly complete depletion of the cortical ER accompanied by a progressive build-up of perinuclear virus-induced ER aggregates. These contained VPg either as polyprotein precursors involved in RNA replication or as a final maturation product associated with viral RNA and also double-stranded viral replicative forms and neosynthesized viral RNA, which confirmed their direct involvement in GFLV replication. The perfect colocalization of dsRNA and neosynthesized RNA signals within ER aggregates, together with the exclusion from these aggregates of the Golgi which remained essentially unaffected, leads us to conclude that the ER is the major contributor to the morphogenesis of the viral compartment where virus replication occurs.

Several plant viruses such as *Brome mosaic virus*, *Tobacco mosaic virus* (TMV), *Tobacco etch virus*, CPMV, and, more recently, *Peanut clump virus* (PCV) were demonstrated to use ER-derived membranes for their replication (11, 17, 50, 51, 59). Like GFLV, these viruses all induced modifications of the ER network but with noticeable differences, suggesting that these viruses use different mechanisms to recruit membranes.

As with GFLV, the cortical ER morphology was highly per-

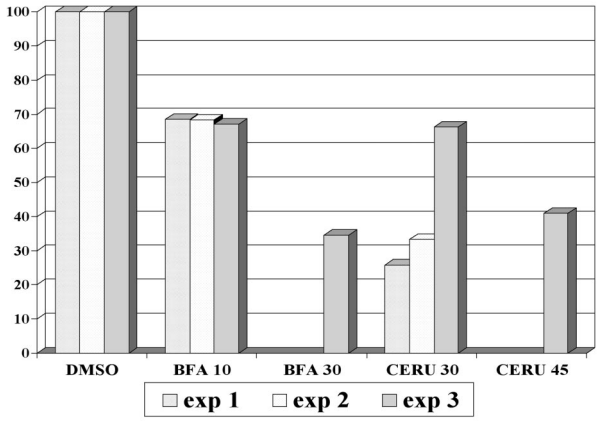

FIG. 5. Effect of BFA and cerulenin on GFLV multiplication in infected T-BY2 protoplasts. Immediately after electroporation of the protoplasts with viral RNA, 10 and 30 μg of BFA/ml or 30 and 45 μM cerulenin (final concentrations) were added, and the protoplasts were further incubated for 48 h. Cell viability was assessed on aliquots of protoplasts by adding 0.1% FDA. The remaining protoplasts were fixed and immunolabeled with anti-VPg or anti-CP antibodies and A568 conjugate. The number of infected cells, as revealed by the anti-VPg or anti-CP signal, was counted versus the total number of protoplasts determined under UV illumination after staining the nucleus with Hoechst 33258 and corrected for cell viability. The results were expressed as the ratio between the percentage of infection and the percentage of viable cells. This ratio was normalized to 100% in the control samples in which only DMSO was added.

turbed in cells infected by tobacco etch virus (59) and TMV (41, 49). For TMV, ER alterations varied with the stage of infection and TMV MP, an integral membrane protein, was demonstrated to be responsible for ER redistribution (49). Both the TMV viral replicase and MP localized to the cytoplasmic face of the cortical ER (30). Although some replication centers were found in the ER-rich perinuclear region, many of them remained peripheral. At the mid stage of infection, large cortical aggregates formed, leading to a completely disrupted cortical ER (49) as for GFLV. In contrast, cortical ER and the GA remained essentially unaffected in cells infected with CPMV (11) and PCV (17), although both viruses induced a massive condensation of the perinuclear ER on which replication occurred. The VPg and the 110K protein of CPMV, both of which are RNA1 encoded and involved in replication, were immunodetected on the condensed ER in plant cells (11), and the 60K VPg precursor was by itself able to induce membrane vesiculation in insect cells (63).

The differences observed between viruses belonging to different families probably reflect subtle specificities of their replication machinery, but it is clear that GFLV replication is most closely related to that of CPMV. Such parallelism is not unexpected since CPMV and GFLV belong to the same family and share many common features, among them a similar genome organization (2).

GFLV RNA replication on ER-derived membranes requires continuous lipid synthesis and functional intracellular vesicle-dependent secretory transport. The physical association of GFLV-encoded proteins involved in replication with ER-derived membranes was further supported by sucrose gradient-ISEM analysis. Bottom fractions enriched in ER rather than Golgi markers contained also the 90- and 73-kDa VPg precursors and electron microscopy of these fractions revealed the presence of numerous membraneous vesicles. These resembled the COP-coated vesicles that traffic between the ER and the GA (1, 47) and were sometimes assembled into "rosettes." Interestingly, similar vesicles and rosettes had been isolated from animal cells infected with poliovirus: rosettes were then shown to harbor transcriptionally active replication complexes bound to smooth membrane vesicles and to contain proteins encoded by the poliovirus P2 genomic region in a membrane-associated form (7). Recently, it was demonstrated that poliovirus vesicles are formed at the ER by the cellular COPII budding mechanism and are thus homologous to vesicles of the anterograde transport pathway (58). In view of the close resemblance between both systems, we suggest that GFLV could use a similar mechanism to recruit membranes for replication purposes. This hypothesis is further substantiated by the fact that BFA, a drug known to disrupt COP vesiculation in animals (21, 33) and plants (52) and to inhibit poliovirus replication (12, 32, 42), also inhibited that of GFLV. As for poliovirus (3, 27) and CPMV (11), but in contrast to TMV (11) or PCV (17), inhibitors of lipid biosynthesis such as cerulenin strongly decreased the replication of GFLV. Therefore, GFLV also probably requires both continuous lipid biosynthesis and a functional secretory transport system, which it modifies and diverts to support its replication, but it is not known so far whether GFLV is also able to inhibit exocytosis.

In conclusion, both de novo synthesis of membranes and endomembrane vesicular trafficking are most probably required for GFLV replication. Future work will focus on identifying which intermediate or final maturation product derived from GFLV polyprotein P1 is responsible for the recruitment of vesicles from the ER and whether this phenomenon occurs through a COP budding mechanism.

Not all GFLV-encoded proteins are associated with the virus-induced ER-derived compartment. GFLV RNA1 supports its own replication (65) and is sufficient to cause the complete cytopathic effect (22) without any protein not involved in replication intervening or being required (23). This is in contrast to TMV, for which the MP is responsible for ER modifications (49). In line with the proposed association of P2 with RNA2 via the 2A region (23), some label corresponding to the movement protein 2B (presumably as the polyprotein or a proteolytic maturation precursor) and the coat protein were occasionally detected in the vicinity of the replication compartment. Coat protein was occasionally detected within the nucleoplasm, but its presence there may not be biologically relevant. Finally, the CP-containing spikes in Fig. 5D could correspond to the intermediate filament-like fibers observed on the electron micrograph. These may be involved in the intracellular transport mechanism of virions and/or MP: indeed, similar structures were observed with another picornavirus, Theiler's murine encephalomyelitis virus, in which physical interaction between virions and intermediate filament components was demonstrated (46). Consistent with its function in cell-to-cell movement, the movement protein was generally detected at the cell periphery at 48 hpi, probably after its release from the precursor polyprotein. In this case, no immunolabeling corresponding to replication-specific proteins was found to localize with it any more. This suggests that MP was transported by a still-

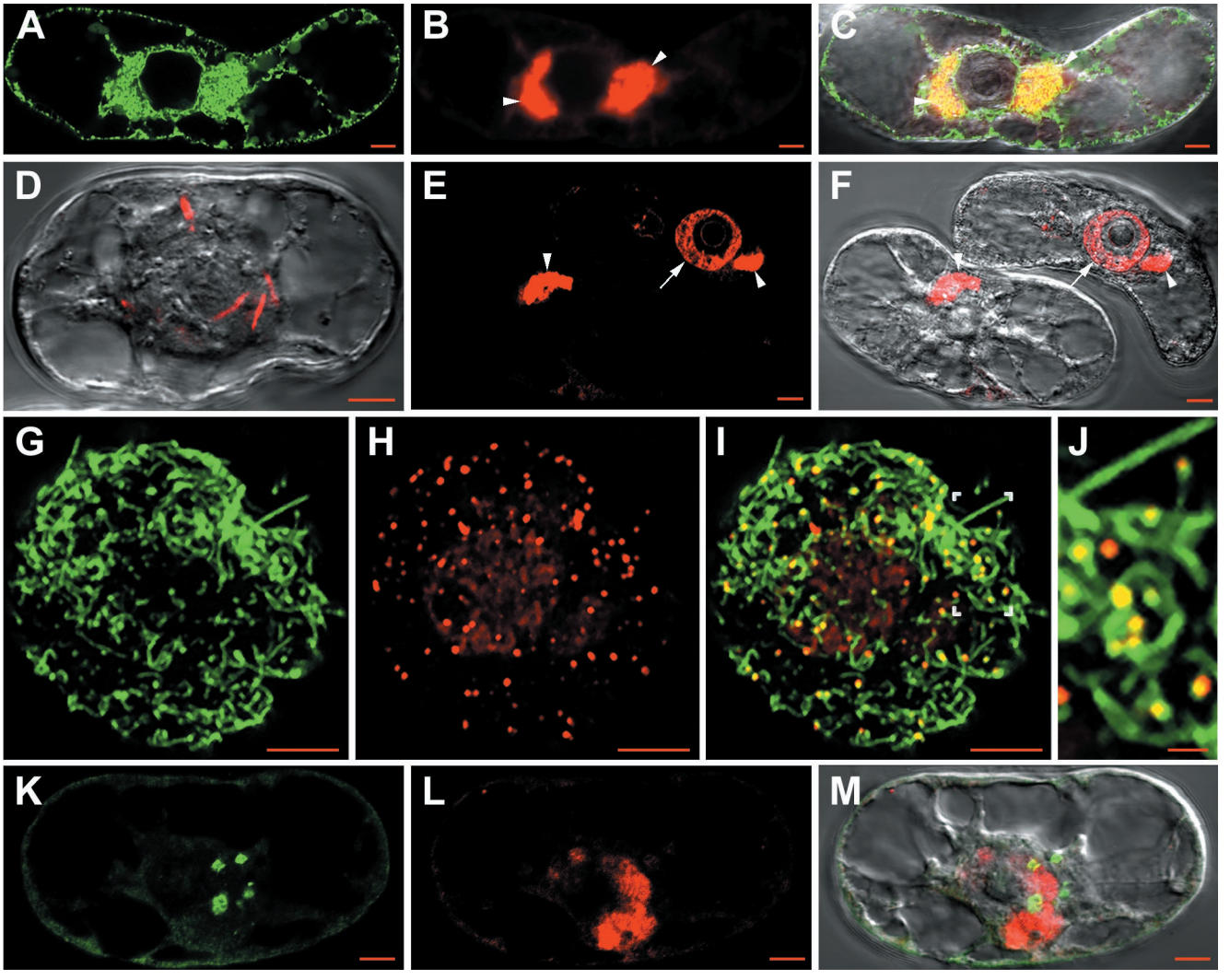

FIG. 6. Confocal immunomicroscopy on healthy or GFLV-infected T-BY2 protoplasts. Cells were from transgenic lines expressing GFP in the ER (A, B, and C) or from wild type (D to M). Cells were harvested at 48 h p.i. and treated as in Fig. 1. Labelings were done with anti-CP/A568 (B, C, D, E, F, H, I, J, L, and M) or anti-MP/A488 (G, I, J, K, and M). Panels C, I, and M are merged pictures from panels A + B, G + H, and K + L, respectively. Differential interference contrast observations were superimposed in panels C, D, F, and M for visualization of the cell and its nucleus. Panel J is a 2.8-fold magnification of the area indicated in panel I. The arrowheads in panels B, C, E, and F indicate the perinuclear viral compartment. The arrows in panels E and F indicate the CP labeling in the nucleoplasm. The boxed region in panel I is shown enlarged in panel J. Bar, 5 μm except in panel J (1 μm).

unknown mechanism to the plasma membrane where it associated with plasmodesmata to form tubules containing virus particles (54; unpublished results). We are currently investigating the mechanism by which GFLV MP is transported intracellularly and whether it moves to the cell periphery alone or in association with virions.

ACKNOWLEDGMENTS

We are grateful to K. Danna and A. Nebenführ, University of Colorado, Boulder, for providing the transgenic T-BY2 cell lines expressing GFP in the ER and the Golgi and to C. Hawes (Oxford, United Kingdom), M. Fuchs (Colmar, France), R. M. Napier (Warwick, United Kingdom), and J.-Y. Lee (Melbourne, Australia) for providing Jim84, anti-CP, anti-HDEL, and anti-dsRNA antibodies, respectively. We are grateful to Moët and Chandon, Epernay, France, for their constant interest in the work and financial support. We thank P. Michler for technical assistance in electron microscopy.

This work was supported by the CNRS and by the Université Louis Pasteur, Strasbourg, France. The interinstitute Zeiss LSM510 confocal microscopy platform was cofinanced by the CNRS, the Université Louis Pasteur, the Région Alsace, the Association de la Recherche sur le Cancer, and the Ligue Nationale contre le Cancer.

REFERENCES

1. **Antonny, B., and R. Scheckman.** 2001. ER export: public transportation by the COPII coach. Curr. Opin. Cell Biol. **13:**438–443.
2. **Argos, P., G. Kamer, M. J. Nicklin, and E. Wimmer.** 1984. Similarity in gene organization and homology between proteins of animal picornaviruses and a plant comovirus suggest common ancestry of these virus families. Nucleic Acids Res. **12:**7251–7267.
3. **Barco, A., and L. Carrasco.** 1995. A human virus protein, poliovirus protein 2BC, induces membrane proliferation and blocks the exocytic pathway in the yeast *Saccharomyces cerevisiae*. EMBO J. **14:**3349–3364.
4. **Bienz, K., D. Egger, and T. Pfister.** 1994. Characterization of the poliovirus replication complex. Arch. Virol. **9:**147–157.
5. **Bienz, K., D. Egger, T. Pfister, and M. Troxler.** 1992. Structural and functional characterization of the poliovirus replication complex. J. Virol. **66:** 2740–2747.

6. **Bienz, K., D. Egger, Y. Rasser, and W. Bossart.** 1983. Intracellular distribution of poliovirus proteins and the induction of virus specific cytoplasmic structures. Virology **131:**39–48.
7. **Bienz, K., D. Egger, M. Troxler, and L. Pasamontes.** 1990. Structural organization of poliovirus RNA replication is mediated by viral proteins of the P2 genomic region. J. Virol. **64:**1156–1163.
8. **Bolten, R., D. Egger, R. Gosert, G. Schaub, L. Landmann, and K. Bienz.** 1998. Intracellular localization of poliovirus plus- and minus-strand RNA visualized by strand-specific fluorescent *in situ* hybridization. J. Virol. **72:** 8578–8585.
9. **Burgyan, J., L. Rubino, and M. Russo.** 1996. The 5′-terminal region of a tombusvirus genome determines the origin of multivesicular bodies. J. Gen. Virol. **77:**1967–1974.
10. **Caliguri, L. A., and I. Tamm.** 1970. The role of cytoplasmic membranes in poliovirus biosynthesis. Virology **42:**100–111.
11. **Carette, J. E., M. Stuiver, J. Van Lent, J. Wellink, and A. Van Kammen.** 2000. Cowpea mosaic virus infection induces a massive proliferation of endoplasmic reticulum but not Golgi membranes and is dependent on *de novo* membrane synthesis. J. Virol. **74:**6556–6563.
12. **Cuconati, A., A. Molla, and E. Wimmer.** 1998. Brefeldin A inhibits cell-free. de novo synthesis of poliovirus. J. Virol. **72:**6456–6464.
13. **David, C., R. Gargouri-Bouzid, and A. L. Haenni.** 1992. RNA replication of plant viruses containing an RNA genome. Prog. Nucleic Acid Res. Mol. Biol. **42:**157–227.
14. **De Graaff, M., and E. M. J. Jaspars.** 1994. Plant viral RNA synthesis in cell-free systems. Annu. Rev. Phytopathol. **32:**311–335.
15. **De Zoeten, G. A., A. M. Assink, and A. Van Kammen.** 1974. Association of cowpea mosaic virus-induced double-stranded RNA in a cytopathological structure in infected cells. Virology **59:**341–355.
16. **Driouich, A., L. Faye, and L. A. Staehelin.** 1993. The plant Golgi apparatus: a factory for complex polysaccharides and glycoproteins. Trends Biochem. Sci. **18:**210–214.
17. **Dunoyer, P., C. Ritzenthaler, O. Hemmer, P. Michler, and C. Fritsch.** 2002. Intracellular localization of the peanut clump virus replication complex in tobacco-BY-2 protoplasts containing GFP-labeled endoplasmic reticulum or Golgi apparatus. J. Virol. **76:**865–874.
18. **Echeverri, A., R. Banerjee, and A. Dasgupta.** 1998. Amino-terminal region of poliovirus 2C protein is sufficient for membrane binding. Virus Res. **54:**217–223.
19. **Egger, D., N. Teterina, E. Ehrenfeld, and K. Bienz.** 2000. Formation of the poliovirus replication complex requires coupled viral translation, vesicle production, and viral RNA synthesis. J. Virol. **74:**6570–6580.
20. **Francki, R. I. B., R. G. Milne, and T. Hatta.** 1985. Atlas of plant viruses. CRC Press, Inc., Boca Raton, Fla.
21. **Fujiwara, T., K. Oda, S., Yokota, A. Takatsuki, and Y. Ikehara.** 1988. Brefeldin A causes disassembly of the Golgi complex and accumulation of secretory proteins in the endoplasmic reticulum. J. Biol. Chem. **263:**18545–18552.
22. **Gaire, F.** 1998. Implication du système endomembranaire dans la replication du virus du court-noué de la vigne (GFLV): rôle de la protéine 2A dans la réplication du RNA2. Ph.D. thesis. Université Louis Pasteur de Strasbourg, Strasbourg, France.
23. **Gaire, F., C. Schmitt, C. Stussi-Garaud, L. Pinck, and C. Ritzenthaler.** 1999. Protein 2A of grapevine fanleaf nepovirus is implicated in RNA2 replication and colocalizes to the replication site. Virology **264:**25–36.
24. **Garnier, M., T. Candresse, and J. M. Bové.** 1986. Immunocytochemical localization of TYMV-coded structural and non-structural proteins by the protein A-gold technique. Virology **151:**100–109.
25. **Garnier, M., R. Mamoun, and J. M. Bové.** 1980. TYMV RNA replication in vivo: replicative intermediate is mainly single stranded. Virology **104:**357–374.
26. **Glauert, A. M.** 1991. Epoxy resins: an update on their selection and use. Eur. Microsc. Anal. **13:**13–18.
27. **Guinea, R., and L. Carrasco.** 1990. Phospholipid biosynthesis and poliovirus genome replication, two coupled phenomena. EMBO J. **9:**2011–2016.
28. **Hatta, T., and R. I. B. Francki.** 1978. Enzyme cytochemical identification of single-stranded and double-stranded RNAs in virus-infected plant and insect cells. Virology **88:**105–117.
29. **Hawes, C. R.** 1985. Conventional and high voltage electron microscopy of the cytoskeleton and cytoplasmic matrix of carrot (*Daucus carota* L.) cells grown in suspension culture. Eur. J. Cell Biol. **38:**201–221.
30. **Heinlein, M., H. S. Padgett, J. S. Gens, B. G. Pickard, S. J. Casper, B. L. Epel, and R. N. Beachy.** 1998. Changing patterns of localization of the tobacco mosaic virus movement protein and replicase to the endoplasmic reticulum and microtubules during infection. Plant Cell **10:**1107–1120.
31. **Horsley, D., J. Coleman, D. Evans, K. Crooks, J. Peart, B. Satiat-Jeunemaitre, and C. Hawes.** 1993. A monoclonal antibody, JIM84, recognizes the Golgi apparatus and plasma membrane in plant cells. J. Exp. Bot. **44:**223–229.
32. **Irurzun, A., L. Perez, and L. Carrasco.** 1992. Involvement of membrane traffic in the replication of poliovirus genomes: effects of brefeldin A. Virology **191:**166–175.
33. **Klausner, R. D., J. G. Donaldson, and J. Lippincott-Schwartz.** 1992. Brefeldin A: insights into the control of membrane traffic and organelle structure. J. Cell Biol. **116:**1071–1080.
34. **Kunze, I., S. Hillmer, G. Kunze, and K. Muentz.** 1995. Brefeldin A differentially affects protein secretion from suspension-cultured tobacco cells (*Nicotiana tabacum*). J. Plant Physiol. **146:**71–80.
35. **Kusov, Y. Y., C. Probst, M. Jecht, P. D. Jost, and V. Gauss-Muller.** 1998. Membrane association and RNA binding of recombinant hepatitis A virus protein 2C. Arch. Virol. **143:**931–944.
36. **Lee, J.-Y., J. A. Marshall, and D. S. Bowden.** 1994. Characterization of rubella virus replication complexes using antibodies to double-stranded RNA. Virology **200:**307–312.
37. **Margis, R., F. Hans, and L. Pinck.** 1993. VPg Northern-immunoblots as a means for detection of viral RNAs in protoplasts or plants infected with grapevine fanleaf nepovirus. Arch. Virol. **131:**225–232.
38. **Margis, R., and L. Pinck.** 1992. Effects of site-directed mutagenesis on the presumed catalytic triad and substrate-binding pocket of grapevine fanleaf nepovirus 24-kDa proteinase. Virology **190:**884–888.
39. **Margis, R., C. Ritzenthaler, J. Reinbolt, M. Pinck, and L. Pinck.** 1993. Genome organization of grapevine fanleaf nepovirus RNA2 deduced from the 122K polyprotein P2 in vitro cleavage products. J. Gen. Virol. **74:**1919–1926.
40. **Margis, R., M. Viry, M. Pinck, and L. Pinck.** 1991. Cloning and in vitro characterization of the grapevine fanleaf virus proteinase cistron. Virology **185:**779–787.
41. **Mas, P., and R. N. Beachy.** 1999. Replication of tobacco mosaic virus on endoplasmic reticulum and role of the cytoskeleton and virus movement protein in intracellular distribution of viral RNA. J. Cell Biol. **147:**945–958.
42. **Maynell, L. A., K. Kirkegaard, and M. W. Klymkowsky.** 1992. Inhibition of poliovirus RNA synthesis by brefeldin A. J. Virol. **66:**1985–1994.
43. **Napier, R. M., L. C. Fowke, C. Hawes, M. Lewis, and H. Pelham.** 1992. Immunological evidence that plants use both the HDEL and KDEL for targeting protein to the endoplasmic reticulum. J. Cell Sci. **102:**262–271.
44. **Nebenführ, A., J. A. Frohlick, and L. A. Staehelin.** 2000. Redistribution of Golgi stacks and other organelles during mitosis and cytokinesis in plant cells. Plant Physiol. **124:**135–151.
45. **Nebenführ, A., L. Gallagher, T. G. Dunahay, J. A. Frohlick, A. M. Masurkiewicz, J. B. Meehl, and L. A. Staehelin.** 1999. Stop-and-go movements of plant Golgi stacks are mediated by the acto-myosin system. Plant Physiol. **121:**1127.
46. **Nédellec, P., P. Vicart, C. Laurent-Winter, C. Martinat, M.-C. Prévost, and M. Brahic.** 1998. Interaction of Theiler's virus with intermediate filaments of infected cells. J. Virol. **72:**9553–9560.
47. **Pimpl, P., A. Movafeghi, S. Coughlan, J. Denecke S. Hillmer, and D. G. Robinson.** 2000. *In situ* localization and in vitro induction of plant COPI-coated vesicles. Plant Cell **12:**2219–2235.
48. **Price, A. C., K.-H. Choi, R. J. Heath, Z. Li, S. W. White, and C. O. Rock.** 2001. Inhibition of β-ketoacyl-acyl carrier protein synthases by thiolactomycin and cerulenin. J. Biol. Chem. **276:**6551–6559.
49. **Reichel, C., and R. N. Beachy.** 1998. Tobacco mosaic virus infection induces severe morphological changes of the endoplasmic reticulum. Proc. Natl. Acad. Sci. USA **95:**11169–11174.
50. **Restrepo-Hartwig, M. A., and P. Ahlquist.** 1996. Brome mosaic virus helicase- and polymerase-like proteins colocalize on the endoplasmic reticulum at sites of viral RNA synthesis. J. Virol. **70:**8908–8916.
51. **Restrepo-Hartwig, M. A., and P. Ahlquist.** 1999. Brome mosaic virus RNA replication proteins 1a and 2a colocalize and 1a independently localizes on the yeast endoplasmic reticulum. J. Virol. **73:**10303–10309.
52. **Ritzenthaler, C., A. Nebenführ, A. Movafeghi, C. Stussi-Garaud, L. Behnia, P. Pimpl, L. A. Staehelin, and D. G. Robinson.** 2002. Reevaluation of the effects of brefeldin A on plant cells using tobacco BY2 cells expressing Golgi-targeted-GFP and COP I antisera. Plant Cell **14:**237–261.
53. **Ritzenthaler, C., M. Pinck, and L. Pinck.** 1995. Grapevine fanleaf nepovirus P38 putative movement protein is not transiently expressed and is a stable final maturation product in vivo. J. Gen. Virol. **76:**907–915.
54. **Ritzenthaler, C., A. C. Schmit, P. Michler, C. Stussi-Garaud, and L. Pinck.** 1995. Grapevine fanleaf nepovirus P38 putative movement protein is located on tubules in vivo. Mol. Plant-Microbe Interact. **8:**379–387.
55. **Rohfritsch, O., A. Poirson, A. Turner, M. J. Gagey, K. Roberts, C. Stussi-Garaud, and T. Godefroy-Colburn.** 1996. A modified form of the alfalfa mosaic virus movement protein induces stressed phenotypes in transgenic tobacco. Can. J. Bot. **74:**939–951.
56. **Rubino, L., and M. Russo.** 1998. Membrane targeting sequences in tombusvirus infections. Virology **252:**431–437.
57. **Rubino, L., F. Weber-Lotfi, A. Dietrich, C. Stussi-Garaud, and M. Russo.** 2001. The open reading frame 1-encoded ('36K') protein of Carnation Italian ringspot virus localizes to mitochondria. J. Gen. Virol. **82:**29–34.
58. **Rust, R. C., L. Landmann, R. Gosert, B. L. Tang, W. Hong, H. P. Hauri, D. Egger, and K. Bienz.** 2001. Cellular COPII proteins are involved in production of the vesicles that form the poliovirus replication complex. J. Virol. **75:**9808–9818.
59. **Schaad, M. C., P. E. Jensen, and J. C. Carrington.** 1997. Formation of plant

RNA virus replication complexes on membranes: role of an endoplasmic reticulum-targeted viral protein. EMBO J. **16:**4049–4059.
60. **Schindler, T., R. Bergfeld, M. Hohl, and P. Schopfer.** 1994. Inhibition of Golgi apparatus function by brefeldin A in maize coleoptiles and its consequences on auxin mediated growth, cell wall extensibility, and secretion of cell wall proteins. Planta **192:**404–413.
61. **Schneider, F., R. Lessire, J. J. Bessoule, H. Juguelin, and C. Cassagne.** 1993. Effect of cerulenin on the synthesis of very-long-chain fatty acids in microsomes from leek seedlings. Biochim. Biophys. Acta **1152:**243–252.
62. **Suhy, D. A., T. H. Giddings, Jr., and K. Kirkegaard.** 2000. Remodeling the endoplasmic reticulum by poliovirus infection and by individual viral proteins: an autophagy-like origin for virus-induced vesicles. J. Virol. **74:**8953–8965.
63. **Van Bokhoven, H., J.W.M. van Lent, R. Custers, J. M. Vlak, J. Wellink, and A. van Kammen.** 1992. Synthesis of the complete 200K polyprotein encoded by cowpea mosaic virus B-RNA in insect cells. J. Gen. Virol. **73:**2775–2784.
64. **van Lent, J., M. Storms, F. van der Meer, J. Wellink, and R. Goldbach.** 1991. Tubular structures involved in movement of cowpea mosaic virus are also formed in infected cowpea protoplasts. J. Gen. Virol. **72:**2615–2623.
65. **Viry, M., M. A. Serghini, F. Hans, C. Ritzenthaler, M. Pinck, and L. Pinck.** 1993. Biologically active transcripts from cloned cDNA of genomic grapevine fanleaf nepovirus RNAs. J. Gen. Virol. **74:**169–174.
66. **Wellink, J., J. van Lent, and R. Goldbach.** 1988. Detection of viral proteins in cytopathic structures in cowpea protoplasts infected with cowpea mosaic virus. J. Gen. Virol. **69:**751–755.